Modeling the role of oxygen vacancy on ferroelectric properties in thin films

Veng Cheong Lo[a)]
Department of Applied Physics, The Hong Kong Polytechnic University, Hunghom, Kowloon Hong Kong, China

(Received 29 May 2002; accepted 20 September 2002)

The presence of oxygen vacancies is considered to be the cause of various phenomena in ferroelectric thin films. In this work, the role of oxygen vacancies is theoretically modeled. Various properties are numerically simulated using the two-dimensional Ising model. In the presence of an oxygen vacancy in a perovskite cell, the octahedral cage formed by oxygen ions is distorted so that the potential energy profile for the displacement of the titanium ion becomes asymmetric. It requires additional energy to move from the lower minimum position to the higher one. Moreover, space charges are also developed by trapping charge carriers into these vacancies. The combination of the pinning effect induced by the distorted octahedral cage and the screening of the electric field in the presence of space charges results in phenomena such as fatigue and imprint. © *2002 American Institute of Physics.* [DOI: 10.1063/1.1520718]

I. INTRODUCTION

Since the development of thin-film fabrication techniques, ferroelectric thin films have been widely used in microelectronic devices, such as superconductor/ferroelectric thin-film tunable microwave components, ferroelectric thin-film waveguides, volatile memory (DRAM), and nonvolatile memory (NVRAM). For the best performance, it is desirable to have a "*square*" and symmetric hysteresis (P–E) loop, long endurance, and low leakage current. In pratice, these qualities cannot always be achieved. In particular, polarization fatigue[1] and imprint[2] are the two degradation problems commonly observed. Previous studies have found that oxygen vacancy is the dominant point defect in oxide ferroelectric thin films.[3] It has also been regarded as the cause of many detrimental effects.[3–6] This has motivated an extensive study of oxygen vacancy in ferroelectric thin films.

The study of oxygen vacancy can be grouped into three categories: (i) its generation, (ii) its effects, and (iii) its characterization. The first category concerns how oxygen vacancies are generated during the formation of ferroelectric films or devices. The formation of metallic electrodes has been traditionally considered as the source of vacancy generation.[7] Doping and nonstoichiometry in thin films are other sources.[8,9] The effects of oxygen vacancy have also been studied extensively. It has been suggested that the oxygen vacancy plays different roles such as pinning domain walls,[10] screening the electric field near the space charge region,[11] impeding the displacement of the Ti^{4+} ion,[11] trapping charge carriers,[12] and enhancing the leakage current.[13] Subsequent phenomena such as fatigue and imprint are associated with these effects. There are also a number of reports on the characterization of oxygen vacancy, using microscopic and optical techniques.[14] Various electrical characterization techniques, including the resistivity change technique,[15] dielectric response,[15] and deep-level-transient spectroscopy (DLTS) (Ref. 16) have also been used.

While there are numerous experimental studies on the effects of oxygen vacancy, quantitative theoretical explanations are still lacking. Among the few theoretical investigations into oxygen vacancy, Dawber and Scott[17] have presented an analytical expression for the oxygen concentration after N switching cycles. They proposed that the fatigued polarization is inversely proportional to the concentration of oxygen vacancies. The fatigue behavior was thus obtained and compared with experiments. However, the authors did not explain how the reciprocal relation was derived. Desu[18] has also simulated the oxygen vacancy-induced fatigue effect by assuming that the charge being trapped per switching cycle is proportional to the change in the defect flux. The decrease of internal field was assumed to be proportional to this flux change. The polarization fatigue was then simulated. Carrico *et al.*[19] have computed ferroelectric thin-film capacitors using Landau free energy. The subsurface space charge induced by oxygen vacancies was included. This has helped to elucidate the effects of microstructures on the device performance. The effects of oxygen vacancies on electrical properties such as low-frequency dielectric relaxation and electric conduction,[20] I–V and C–V characteristics of metal–ferroelectric–semiconductor field-effect transistors (MFSFETs),[21] and leakage current[22] have also been simulated.

There are also a number of experimental reports on the effect of oxygen vacancies on the P–E hysteresis loop. Numerical simulation of this loop in the presence of oxygen vacancies is still rare. In this article, the effect of the oxygen vacancy on the displacement of Ti^{4+} in a perovskite-type ferroelectric thin film will be discussed. This effect is mathematically modeled by an additional term in the system Hamiltonian. The trapping of charge carriers by oxygen vacancies will also be considered and the imprint and polarization fatigue simulated.

[a)]Electronic mail address: apavclo@polyu.edu.hk

 © 2002 American Institute of Physics

Downloaded 01 Apr 2011 to 158.132.161.9. Redistribution subject to AIP license or copyright; see http://jap.aip.org/about/rights_and_permissions

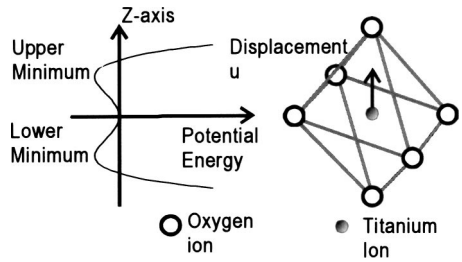

FIG. 1. Potential energy profile for the displacement of the titanium ion along the thickness direction (ordinate) is shown on the left. The symmetric (with respect to the horizontal plane) octahedral cage is shown on the right. There are two equally weighted potential minima for Ti^{4+} located at the top and the bottom of the central plane, respectively.

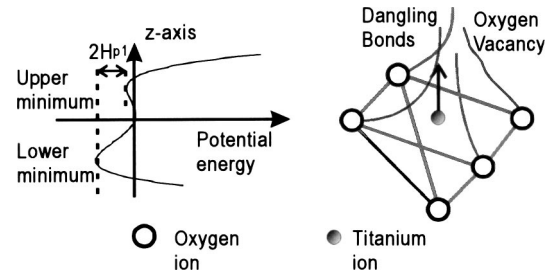

FIG. 2. The asymmetric potential profile in the presence of an oxygen vacancy at the top of the cage is shown on the left. The distorted octahedral cage and the dangled bonds are shown on the right. It requires additional energy $2\Delta H_{P1}$ for Ti^{4+} located at the bottom minimum site to displace to the upper one.

II. THEORY AND MODELING

In this model simulation, a single-crystalline thin film of perovskite-type ferroelectric material, such as lead zirconium titanate with a crystal orientation along the (100) direction, is considered. Below the Curie temperature, it is in tetragonal phase and the elongated edge is along the thickness direction (or the z direction). The Ti^{4+} ion in the octahedral site also displaces along the z direction. In the absence of an oxygen vacancy, the octahedral cage formed by the six oxygen ions is slightly stretched along the z direction and symmetric with respect to the XY plane. According to Landau theory, if the displacement of Ti^{4+} is treated as the order parameter u, then the system free energy can be expressed in terms of the power series of this order parameter. Because of the symmetric property, only terms with even-number indices appear. There are two off-centered potential minima on opposite sides of the central position, as shown in Fig. 1. These minima are equilibrium positions for the Ti^{4+} ion. They are called top and bottom minimum sites, respectively, according to their positions relative to the center of the cage. The probabilities of displacing Ti^{4+} from any one of these minima to the other are equal. This displacement is associated with dipole switching, visualized as the flipping of a *pseudospin* between $+z$ and $-z$ directions.

In the presence of an oxygen vacancy at the top of the octahedral cage, the cage is distorted. The four bonds connecting between the top vertex of the cage and the other four oxygen ions are dangled. Because of Coulombic interaction, Ti^{4+} moves favorably toward the bottom minimum site. The free-energy profile now becomes asymmetric: the value at the bottom minimum site is lower than that at the top, as shown in Fig. 2. It is possible to displace Ti^{4+} from the bottom minimum site to the top, with the expense of additional energy $2H_{P1}$. This asymmetry implies that terms of odd-number indices must appear in the free-energy expression. In the following calculation, for simplicity, we consider only the contribution from the linear term.

The vacancy can, of course, be located at other positions in the cage. When it is at the bottom vertex, then the free energy profile can be obtained by simply flipping the profile in Fig. 2 vertically. When the vacancy is on one of the vertical planes of the cell, it can be shown that Ti^{4+} is restricted in the central position. The resultant dipole moment in this case is zero. Considering that the concentration of oxygen vacancies is dilute, there is at most one vacancy in each cage. The defect complexes formed by vacancy–vacancy couples or vacancy–impurity couples are also ignored for simplicity.

Considering a two-dimensional film of size $d_x \times d_z$ along the x and z directions, the position of a cell (and, hence, dipole moment or spin) located at (x,z) in the film can be discretized as follows:

$$x = ix_0, \tag{1}$$

$$z = jz_0, \tag{2}$$

where x_0 and z_0 are the sizes of the cell along the x and the z directions, respectively. The dimensions of the film d_x and d_z can then be related by

$$d_x = N_x x_0, \tag{3}$$

and

$$d_z = N_Z z_0, \tag{4}$$

where N_x and N_z are the numbers of cells of the film along x and z directions, respectively. It then becomes a two-dimensional array of cells $(N_x \times N_z)$. The displacement of Ti^{4+} in the (i, j) cell is denoted by u_{ij}. The associated dipole moment is p_{ij}, where $p_{ij} = qu_{ij}$, and q is the electron charge. The film can thus be represented by the two-dimensional array of *pseudospins*, denoted by S_{ij} where $p_{ij} = p_0 S_{ij}$ and p_0 is the dipole moment of each cell when Ti^{4+} displaces to one of the equilibrium positions. S_{ij} has only two values: either $+1$ for upward displacement or -1 for downward displacement.

For simplicity, we consider the effects of the oxygen vacancy located only either at the top or the bottom of the octahedral cage ignoring the contribution from oxygen vacancies at the other positions. The presence of an oxygen vacancy in the cell at a position (i,j) can be mathematically represented by a parameter V_{ij} such that

$$V_{ij} = \begin{cases} -1 & \text{top} \\ +1 & \text{bottom} \\ 0 & \text{otherwise} \end{cases}. \tag{5}$$

Physically, oxygen vacancies are generated from outside through the electrodes, thus there must be a distribution

Downloaded 01 Apr 2011 to 158.132.161.9. Redistribution subject to AIP license or copyright; see http://jap.aip.org/about/rights_and_permissions

function for vacancy concentration that has maximum values at the two interfaces and decays gradually into the interior of the film. This function can be expressed as

$$f(z)=\alpha[\exp(-z/Lz_1)+r\exp(-(d_z-z)/Lz_2)], \tag{6}$$

where L_{z1} and L_{z2} are the characteristic diffusion lengths at the top and bottom interfaces, respectively. The parameters r and α are given as

$$r=\frac{R_v-\exp(-d_z/L_{z1})}{1-R_v\exp(-d_z/L_{z2})},$$

and

$$\alpha=\frac{1}{L_{z1}\{1-\exp(-d_z/L_{z1})+L_{z2}r[1-\exp(-d_z/L_{z2})]\}}, \tag{7}$$

respectively, where $R_v=f(d_z)/f(0)$ gives the ratio of vacancy concentrations at the two interfaces. The distribution function is normalized such that $\int_0^{d_z}f(z)dz=1$ ensures that the same quantity of oxygen vacancies is obtained even by varying L_{z1} or L_{z2}.

The quantity of oxygen vacancies at the top electrode can be represented by a parameter R_P such that the number of oxygen vacancies there is given by R_PN_x. Likewise, the number at the bottom electrode $(z=d_z)$ is $R_PR_vN_x$. The two-dimensional distribution of oxygen vacancies are then generated randomly according to the ratios R_P, R_V and the distribution function $f(z)$ using Monte Carlo simulation.

As has been mentioned before, in the presence of an oxygen vacancy at the top of the cage located at the position (i ,j) $(V_{ij}=-1)$, additional energy $2H_{p1}$ is required to displace Ti^{4+} from the lower minimum site to the upper one. The expression of this additional energy term is given by

$$H_a=-H_{p1}V_{ij}S_{ij}. \tag{8}$$

If, initially, Ti^{4+} is located at the lower minimum site $(S_{ij}=-1)$, then the system Hamiltonian is $H^{(i)}=H_0+H_a^{(i)}$, where H_0 is the Hamiltonian in the absence of the oxygen vacancy, $H_a^{(i)}=-H_{p1}$. Similarly, the system Hamiltonian in the final stage is $H^{(f)}=H_0+H_a^{(f)}$, where $H_a^{(f)}=H_{p1}$. The change in Hamiltonian by flipping the downward dipole to an upward direction is then $\Delta H=H^{(f)}-H^{(i)}=2H_{p1}$. Likewise, one can prove that an amount of energy released by flipping the upward dipole to a downward one is $-2H_{p1}$.

The distortion of the cage in the presence of the oxygen vacancy also induces an additional energy term from the couplings of this distorted cage with the neighboring dipoles as follows:

$$H_b=-\sum_{i'j'}H_{p2}V_{ij}S_{ij}S_{i'j'}, \tag{9}$$

where $S_{i'j'}$ is the *pseudospin* state of one of the neighboring dipoles. The system Hamiltonian can thus be expressed as

$$\begin{aligned}H&=-J\sum_{ij}\sum_{i'j'}S_{ij}S_{i'j'}-p_0\sum_{ij}S_{ij}E_j+H_a+H_b,\\&=-J\sum_{ij}\sum_{i'j'}S_{ij}S_{i'j'}-p_0\sum_{ij}S_{ij}E_j-H_{p1}\sum_{ij}V_{ij}S_{ij}\\&\quad-H_{p2}\sum_{ij}\sum_{i'j'}V_{ij}S_{ij}S_{i'j'},\end{aligned} \tag{10}$$

where J is the coupling coefficient between neighboring dipoles. It will be shown later that the coupling effect is isotropic. E_j is the electric field at a depth z along the thickness direction. The summations in Eq. (10) are over all the nearest neighbors only. Furthermore, in the presence of a space charge distribution, the spatial variation of the electric field is governed by the Poisson equation:

$$\frac{d^2\phi}{dz^2}=-\frac{Q_s(z)}{\varepsilon_s}, \tag{11}$$

and

$$E(z)=E(jz_0)=E_j=-\frac{d\phi}{dz}, \tag{12}$$

where $Q_s(z)$ is the space charge distribution and ϕ the electrical potential. The boundary conditions for the potentials at the two interfaces are $\phi(0)=0$ and $\phi(d_z)=V_a(t)$, where $V_a(t)=V_0\sin(2\pi t/T_R)$ is the externally applied voltage with an amplitude V_0 and a period T_R. In order to generate *P–E loops*, we defined an average electric field by $E_{\mathrm{av}}=-V_a(t)/d_z$ for the abscissa. The polarization of the whole film is given by

$$P=\frac{\Sigma_{ij}p_{ij}}{d_xd_z}. \tag{13}$$

Finally, assuming that the space charge is generated by the trapping of holes or the emission of electrons by oxygen vacancies, then $Q_s(z)$ follows the same distribution of oxygen vacancies such that $Q_s(z)=q_rf(z)$, where the distribution function $f(z)$ is given by Eq. (6), and the charge concentration by q_r.

All necessary equations having been formulated, they are then converted into expressions of dimensionless variables. The definitions of these variables are shown as follows:

$$\begin{aligned}&\tilde{H}=H/J,\ \ \tilde{H}_{P1}=H_{P1}/J,\\&\tilde{H}_{P2}=H_{P2}/J\ \ \tilde{E}_j=E_jp_0/J,\\&\tilde{L}_{Z1}=L_{Z1}/z_0\ \ \tilde{L}_{z2}=L_{Z2}/z_0,\ \ \tilde{d}_z=d_z/z_0,\end{aligned} \tag{14}$$

where all dimensionless variables are denoted by the tilde "~" over them. The polarization, potential, and space charge concentration q_r are normalized by

$$\tilde{P}=x_0z_0P/p_0,\ \ \tilde{\phi}=\frac{\phi p_0}{Jz_0},\ \ \tilde{q}_r=\frac{q_rp_0z_0}{\varepsilon_sJ}. \tag{15}$$

Downloaded 01 Apr 2011 to 158.132.161.9. Redistribution subject to AIP license or copyright; see http://jap.aip.org/about/rights_and_permissions

After the transformation, the dimensionless system Hamiltonian can be obtained as follows:

$$\tilde{H}=-\sum_{ij}\sum_{i'j'}S_{ij}S_{i'j'}-\sum_{ij}\tilde{E}_jS_{ij}-\tilde{H}_{p1}\sum_{ij}V_{ij}S_{ij}$$
$$-\tilde{H}_{p2}\sum_{ij}\sum_{i'j'}V_{ij}S_{ij}S_{i'j'}. \quad (16)$$

The Poisson equation and the electric field distribution are transformed into

$$\frac{d^2\tilde{\phi}}{d\tilde{z}^2}=-\tilde{q}_r f(\tilde{z}), \quad (17)$$

and

$$\tilde{E}=-\frac{d\tilde{\phi}}{d\tilde{z}}. \quad (18)$$

Equations (17) and (18) were solved by the Gauss elimination method. In this model calculation, the distribution function is assumed static. The electric field distribution obtained in such a way is independent of the spin configuration of the film. This assumption is only for simplification purposes. In general, complications may arise in such a way that the space charge depends both on time and local polarization (or electric field).

The normalized temperature is given by $\tilde{T}=kT/J$. It is beyond our scope to find the Curie temperature $\tilde{T}_C$ in our system. A theoretical value of $\tilde{T}_C=2.269$ has been suggested for a two-dimensional Ising model.[23] The value of $\tilde{T}$ was restricted to below 2.269 in our present calculation. The normalized time is related by $\tilde{t}=t/t_0=(\mathrm{MSC})$; where t_0 is the time step for each Monte Carlo step, and MCS is the number of Monte Carlo steps. The period and frequency are normalized as $\tilde{T}_R=T_R/t_0$ and $\tilde{f}=1/\tilde{T}_R=f.t_0$, respectively.

In order to simulate a film with infinite surface area but finite thickness, a periodic boundary is adopted along the transverse direction (x axis), while a free boundary condition is chosen at the two interfaces. These conditions can be expressed mathematically by the following equations:

$$S_{0,j}=S_{N_X,j},\ \ S_{N_X+1,j}=S_{1,j},$$

and (19)

$$S_{i,0}=S_{i,N_z+1}=0.$$

As in the conventional Ising model, *pseudospin* $S_{k,m}$ at an arbitrary site (k,m) in the film is chosen at random and the flipping of this spin is tested by the following algorithm; the change in Hamiltonian after flipping this spin is evaluated by the following expression:

$$\Delta\tilde{H}=2\{(S_{k,m+1}+S_{k,m-1}+S_{k+1,m}+S_{k-1,m})+\tilde{E}_k\}S_{k,m}$$
$$+\tilde{H}_{p1}V_{k,m}S_{k,m}+\tilde{H}_{p2}|V_{k,m}|S_{k,m}(S_{k,m+1}+S_{k,m-1}$$
$$+S_{k+1,m}+S_{k-1,m}). \quad (20)$$

A random number R is generated such that $0<R<1$. Flipping is allowed under the following conditions: (i) $\Delta\tilde{H}<0$, or (ii) $\exp(-\Delta\tilde{H}/\tilde{T})>R$. The spin configuration $\{S_{ij}\}$ is updated after each MSC, and the overall polarization can be obtained from the following expression:

$$\tilde{P}=\frac{\Sigma_{ij}S_{ij}}{N_xN_z}. \quad (21)$$

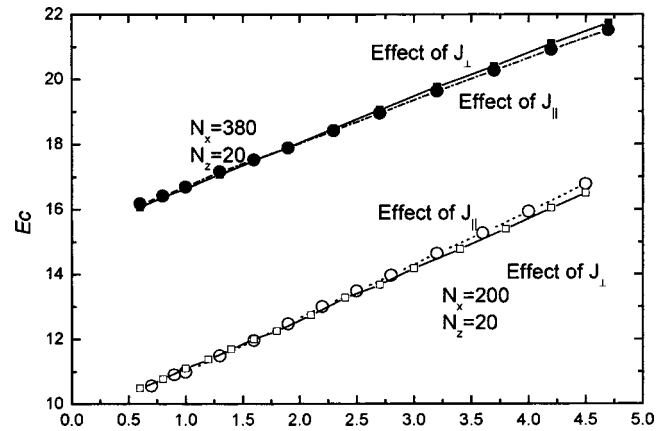

FIG. 3. Effect of coupling coefficients along different directions on the coercive field: the variation of $J_\perp$ while keeping $J_\parallel$ constant are shown by solid lines with squares; the variation of $J_\parallel$ with $J_\perp$ fixed by dotted lines with circles. Open symbols are for the film size: 200×20; solid symbols are for 380×20. The abscissa represents the value of coupling coefficients.

III. RESULTS AND DISCUSSION

We have introduced some parameters in the previous section, which can be determined by fitting particular experimental results. However, in order to maintain the generality, they are kept as free parameters. We have adopted the following numerical values for these parameters: $N_x=200$, $N_z=20$, $z_0=0.01$, $t_0=0.25$, $\tilde{T}=1.85$, $\tilde{H}_{P1}=5$, $\tilde{H}_{P2}=2$, $R_p=0.6$, $R_V=0.65$, $\tilde{L}_{z1}=0.08$, $\tilde{L}_{Z2}=0.075$, $\tilde{d}_z=0.2$, $\tilde{V}_0=2.5$, $\tilde{T}_R=20000$, and $\tilde{q}_r=5$, except when the effect of the individual parameter is being studied.

As mentioned above, the coupling coefficient J is isotropic. By testing this assumption, different coupling coefficients, $J_\perp$ along the thickness direction and $J_\parallel$ along the transverse direction, are defined. Their effect on coercive field E_C was investigated by varying one coupling coefficient while keeping the other fixed. As shown in Fig. 3, there are two lines in each group. Open symbols denote the results from a film of size 200×20, while solid symbols are for 380×20. Squares and solid lines are for the variation of $J_\perp$, while circles and dotted lines are for the variation of $J_\parallel$. There is no pronounced difference between the variation of $J_\perp$ and that of $J_\parallel$, thus it can be concluded that the coupling coefficient is isotropic: $J=J_\perp=J_\parallel$.

The validity of this theoretical formulation has been tested by investigating the effects of temperature, frequency, and amplitude of the driving voltage. The conclusion with regard to these effects has been well established both experimentally and theoretically.[10,24] Generally speaking, both the loop area and the coercive field are increased by either the amplitude or frequency, or both. Conversely, both of them

Downloaded 01 Apr 2011 to 158.132.161.9. Redistribution subject to AIP license or copyright; see http://jap.aip.org/about/rights_and_permissions

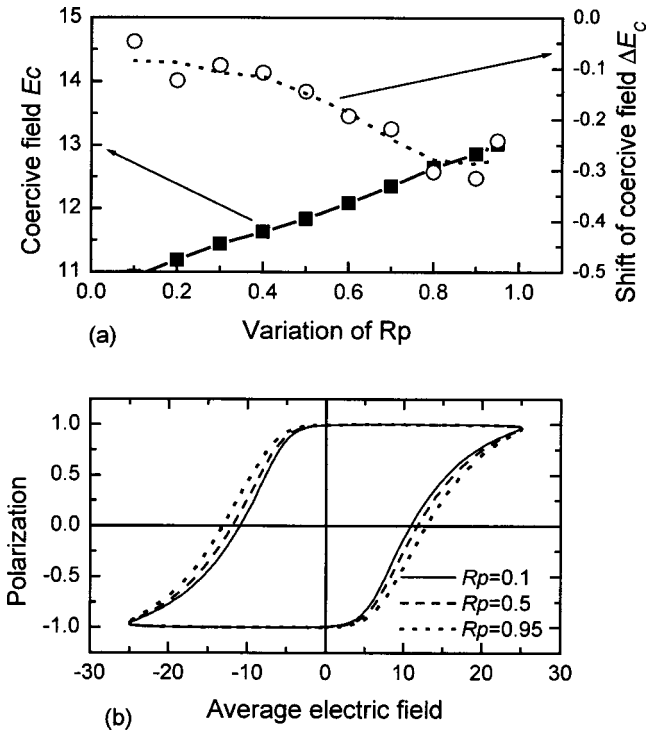

FIG. 4. Effect of the portion of cells at the surface when oxygen vacancies are present, denoted by R_P. There are pronounced increases in coercive field and drift in P–E loop (toward the left) (a). P–E loops for different values of R_p:0.1, 0.5 and 0.95, are shown in (b).

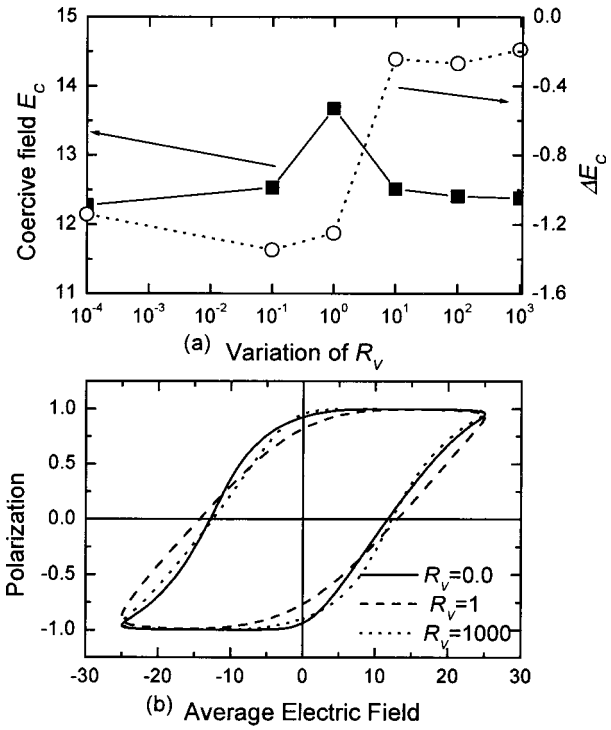

FIG. 5. Effect of the ratio of oxygen vacancy concentrations at the bottom surface to the top one, denoted by R_V. (a) It is noted that the coercive field is maximum for a symmetric distribution ($R_V=1$). P–E loops for three different distributions: oxygen vacancies concentrated at the top surface (solid line: $R_V=0.0$); symmetric distribution (dash line: $R_V=1.0$); and oxygen vacancies concentrated at the bottom surface (dotted line: $R_V=1000$) (b).

are reduced by increasing the temperature as the "*hardness*" of the ferroelectricity is reduced by thermal energy. Our simulation results agree with these features.

In addition to the above, the effects induced by different parameters characterizing oxygen vacancies were also studied and the results are presented in the following.

A. Effect of R_P

Parameter R_P represents the portion of cells at the top electrode/film interface where oxygen vacancies exist. Figure 4 shows the different P–E loops for $R_P=0.1$, 0.5, and 0.95, respectively. It is revealed that coercive field E_C increases with R_P while there is no pronounced effect on the remanent polarization. The enhancement of the coercive field by R_p implies an increase in polarization *hardness* due to the presence of oxygen vacancies. The origin of this enhancement is that an additional energy is required for the displacement of Ti^{4+} in the presence of an oxygen vacancy in the cell. Moreover, there is a slight shifting of the coercive field ($\Delta E_C = E_{C1} - E_{C2} < 0$) toward the left-hand side of the electric field axis on increasing R_p, because the vacancy distribution is asymmetric. Increasing R_P means increasing the influence of oxygen vacancies.

B. Asymmetric distribution of oxygen vacancies

There are two ways to characterize the asymmetric distribution. As shown in Eqs. (6) and (7), if the value R_V is larger than 1, then the vacancy concentration at the bottom electrode exceeds that at the top electrode. If R_V is less than 1, the reverse condition holds. This inequality in vacancy concentrations is caused by the different electrodes causing a difference in film/electrode interfaces. The different ways of incorporating the electrodes also create this inequality. The inequality in diffusion characteristic lengths, i.e., $L_{Z1} \neq L_{Z2}$ also creates an asymmetric distribution. We can investigate this effect by varying L_{Z1} while keeping L_{Z2} constant. Unlike R_V, for a large L_{z1}, not only the oxygen vacancies at the interfaces, but also those deep inside the film, contribute to the switching effects.

The effect of R_V is shown in Figs. 5(a) and 5(b). When $R_v=1$, it is a symmetric case and the hysteresis loop is also symmetric. For other values, the loop shapes become asymmetric. Moreover, the imprint effect as measured by ΔE_C changes from a large negative value to a small one. This means the imprint effect is most serious if the distribution is weighted heavily at the top electrode. There is only a slight effect on the coercive field except when $R_V=1$ where the coercive field is largest.

The effect of L_{Z1} is shown in Figs. 6(a) and 6(b). The coercive field increases with L_{Z1}, reflecting that the oxygen vacancies deep beneath the surface have more influence on the polarization switching. The imprint effect ΔE_C on varying $Lz1$ is also shown: the magnitude of ΔE_C increases with L_{Z1}. We have also investigated the effect of L_{Z2}, which produces similar effects on E_C and ΔE_C as for the variation of L_{Z1}, but with a much lesser extent. This result is consistent with the effect of R_V that oxygen vacancies at the top electrode have more effect on imprint.

Downloaded 01 Apr 2011 to 158.132.161.9. Redistribution subject to AIP license or copyright; see http://jap.aip.org/about/rights_and_permissions

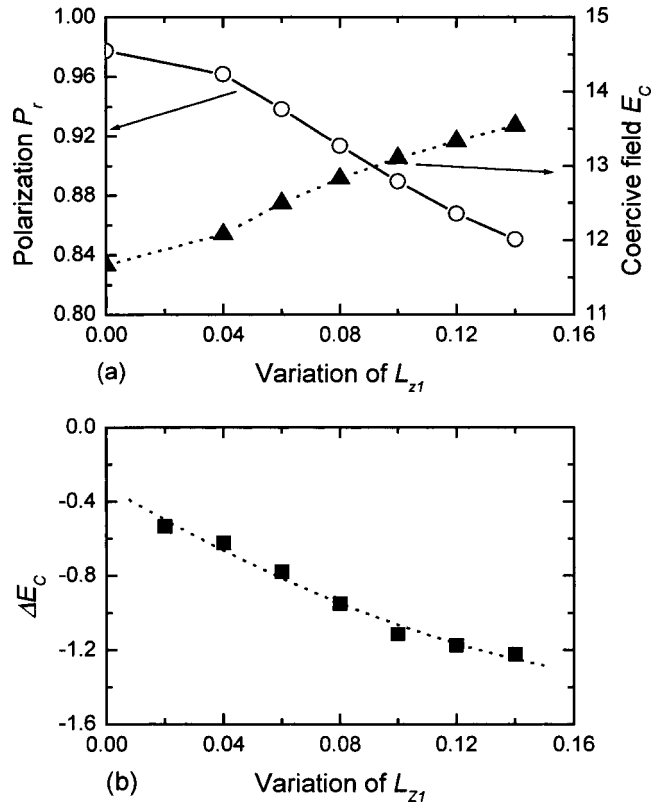

FIG. 6. Effect of variation of the diffusion length L_{Z1} on (a) remanent polarization P_r and coercive field E_c; (b) drift of P–E loop (negative sign for drifting toward the left).

There are quite a number of experimental reports on the effect of oxygen vacancies on the imprint. Friessnegg *et al.*[25] have characterized oxygen-vacancy profiles in a $La_{0.5}Sr_{0.5}CoO_3/Pb_{0.9}La_{0.1}(Zr_{0.2}Ti_{0.8})O_3/La_{0.5}Sr_{0.5}CoO_3$ system using a positron beam. The asymmetric defect profile, which was induced by the cooling of the pulsed laser deposition film under an oxygen deficient ambient, is related to the voltage offset in the P–V loop. It has been suggested that these defects, under a strongly oxygen deficient ambient, are metal ion–vacancy complexes, or isolated oxygen vacancies as well. Several authors have also suggested the space charge developed by the trapping of carriers in these oxygen vacancies is responsible for the imprint effect.[18,25,26]. The presence of an oxygen vacancy, therefore, impedes the displacement of Ti^{4+}. It also traps charge that influences the electric field distribution along the film. The asymmetric distribution of oxygen vacancies creates the imprint effect. The relation between the space charge and oxygen vacancy will be present below.

C. Effect of space charge

The effect of space charge can be simulated by varying parameter $\tilde{q}_r$. It is assumed that the space charge and oxygen vacancies follow the same distribution function defined in Eq. (17). $\tilde{q}_r$ represents the normalized space charge concentration at the top electrode; the value at the bottom electrode is then $R_V\tilde{q}_r$. It is further assumed, for simplicity, that the distribution function is invariant in time. The transport equation of oxygen vacancies must be solved in order to obtain the temporal evolution of the distribution function.

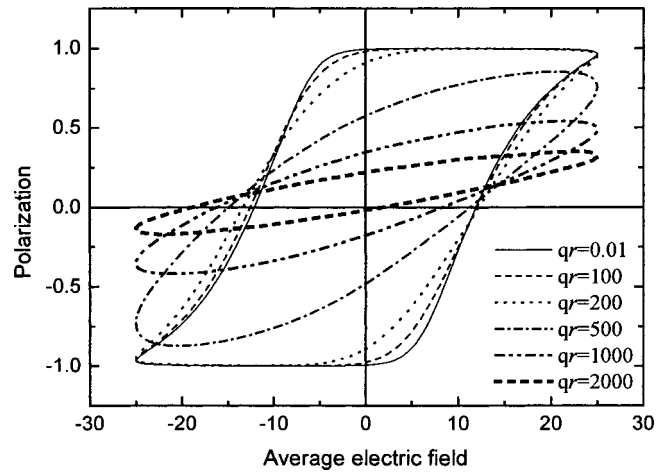

FIG. 7. Effect of the quantity of space charge q_r on the P–E loop. The reduction of remanent polarization and shifting of the loop are quite pronounced for high q_r values.

The effect of $\tilde{q}_r$ values on the P–E loops is shown in Fig. 7. It is obvious that the remanent polarization is significantly reduced by large $\tilde{q}_r$ values (>200). Moreover, the P–E loop shifts toward the left-hand side on increasing $\tilde{q}_r$. This is consistent with the previous suggestion that the development of the space charge enhances the imprint effect.

The spatial distributions of the electric field and the polarization across the film when a maximum positive biasing voltage is applied to the top electrode (at $\tilde{t}=14\,800$) are plotted in Fig. 8. Similar profiles for a maximum negative biasing voltage are plotted in Fig. 9 ($\tilde{t}=25\,900$). Both the electric field and polarization profiles are essentially uniform and follow the sign of the external biasing voltage when the

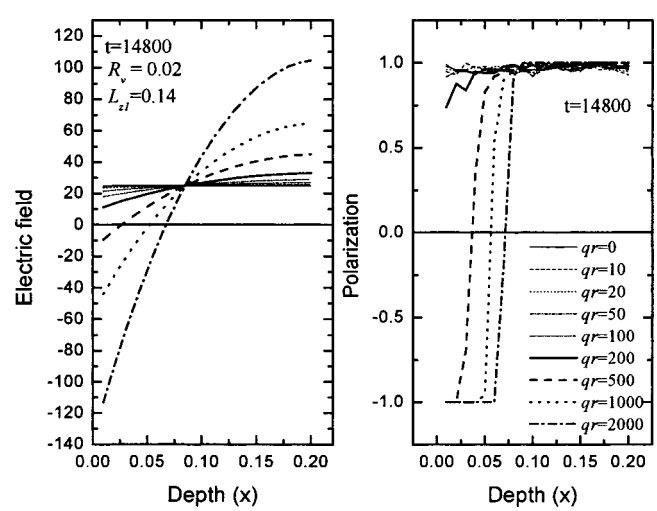

FIG. 8. Distribution profiles of electric field (left) and polarization (right) across the film for different space charge quantities during a positive-biasing voltage. The electric field and polarization are highly nonuniform for q_r500. The electric field and polarization at the top surface layer remain negative, even when the biasing voltage is positive. The parameters for producing these profiles are: $R_V=0.02$, $L_{Z1}=0.14$; the other parameters are the same as those given in the text.

Downloaded 01 Apr 2011 to 158.132.161.9. Redistribution subject to AIP license or copyright; see http://jap.aip.org/about/rights_and_permissions

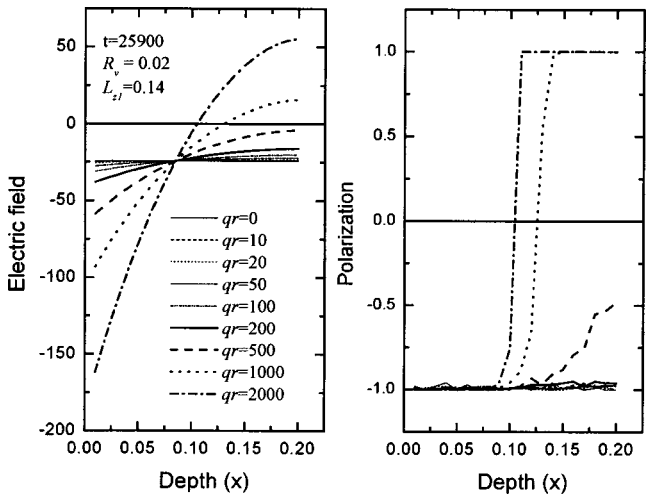

FIG. 9. Distribution profiles of electric field (left) and polarization (right) across the film for different space charge quantities during a negative-biasing voltage. Unlike in Fig. 8, the electric field and polarization at the bottom surface layer remain positive even when the biasing voltage is negative. The adopted parameters are the same as for Fig. 8.

value of $\tilde{q}_r$ is less than 100. Nonuniformity of the profiles appears for $\tilde{q}_r$ larger than 100. Moreover, there are regions where both the electric field and polarization always remain in negative values at the top electrode, and positive values at the bottom electrode, regardless of the sign of the external driving voltage. These regions have been designated *dead layers*,[27] or nonswitching layer,[28] within which the dipoles are not switchable. The size effect of different ferroelectric properties has been attributed to the presence of these layers.[29] It has also been suggested that depolarizing fields exist in these layers. The sense of depolarizing manifests in the opposite direction with respect to the field inside the film. However, in our present simulation, the directions of electric fields within these layers are essentially static, irrespective of the direction of the external driving field.

The P–E loops of the different layers of the films: top electrode, central plane, and bottom electrode, are plotted in Figs. 10(a), 10(b), and 10(c), respectively, under a high space charge concentration $\tilde{q}_r = 500$. The overall P–E loop is also shown in Fig. 10(d). It is clear that the polarization at the top electrode remains negative all the time. The P–E loop at the bottom electrode is severely distorted, the polarization being strongly biased to a positive value. The P–E loop at the central plane is slightly asymmetric. The overall loop shown in Fig. 10(d) exhibits quite a large extent of asymmetry and distortion. Of course, this description strongly depends on the spatial distribution and the space charge concentration. It is also worth mentioning that, unlike the assumptions made in many previous models, the material properties of these *dead* layers are completely identical to those of the rest of the film, except for the presence of the space charge. The presence of the high built-in field due to the space charge already establishes the *dead layers* where the polarization state is static.

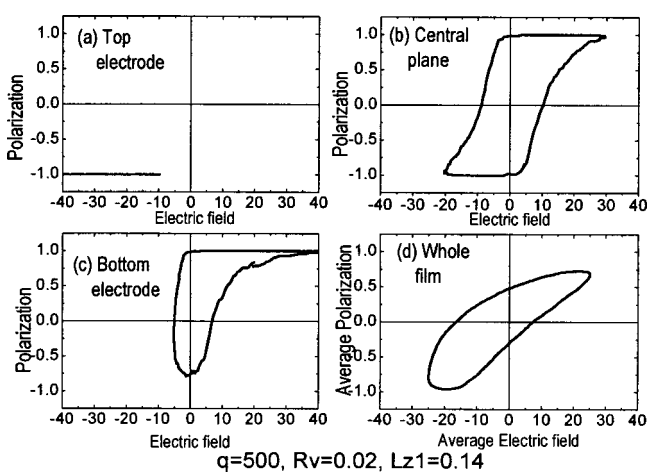

FIG. 10. P–E loops at the (a) top surface, (b) central plane, and (c) bottom surface. Overall P–E loop for the whole film is shown in (d).

Different explanations have been suggested as the causes of polarization fatigue, including damage-induced stress, domain-wall pinning, and the presence of the space charge. Experimental evidence supports that the occurrence of fatigue is closely related to the presence of the space charge. Strontium bismuth tantalate (SBT) film has been considered to be fatigue free. Al-Shareef *et al.*[30] have induced polarization fatigue in SBT film under a $+0.8$ V bias and UV light illumination, where the role of the UV illumination was to generate charge carriers. These carriers were then trapped by vacancies, resulting in space charge regions at the interfaces. Consequently, polarization fatigue behavior appeared in the SBT film in the presence of space charge, as it did in PZT. What is different in SBT film is actually the way of charge generation. For the PZT film, both electrical injection and optical excitation can efficiently create charge carriers in the film. For SBT, only the latter can generate an appreciable amount of charge.

It has been demonstrated before that the presence of uncharged oxygen vacancies does not reduce the remanent polarization very much, either by increasing the factor R_p or L_{Z1} or both. The pronounced polarization suppression effect can, however, be induced by the trapping of charge. It is suggested that the amount of space charge increases with the number of switching cycles N, given by the following relation:

$$\tilde{q}_r = \beta\sqrt{N}. \tag{22}$$

As shown in Fig. 7, the decrease in remanant polarization is associated with the increase of the space charge. The relations of remanant polarization P_r and space charge against N are plotted in Fig. 11, with the parameter $\beta = 0.0316$.

The question remains as to what is the sign of the space charge and what type of charge carriers are trapped during the fatigue process. The fatigue result does not give the answer, because a large built-in field near the interface can be induced not only by a negative space charge region but also by a positive one. This large built-in field reduces the effective field inside the film, making the polarization switching more difficult. On the other hand, if the space charge distribution is nonuniform, then the drifting direction of the P–E loop will depend on the sign of the space charge. In our

Downloaded 01 Apr 2011 to 158.132.161.9. Redistribution subject to AIP license or copyright; see http://jap.aip.org/about/rights_and_permissions

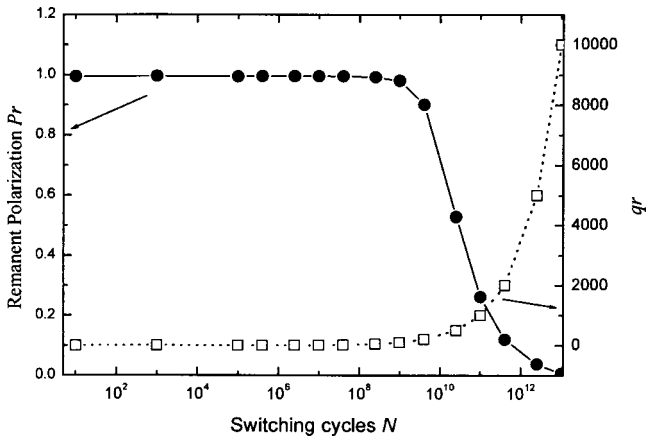

FIG. 11. Reduction of remanent polarization fatigue (solid line and solid cicles) and the accumulation of space charge (dotted line and open squares) as a function of switching cycles.

present simulation, we adopted a sign convention that the top electrode is grounded and the bottom one biased by a driving voltage $V_a(t)$. The electric field has a positive sign if it is directed from the top to the bottom electrode. Thus, the biasing voltage and the average electric field are of opposite signs related by $E_{\mathrm{av}}^{-}=-V_a/d_z$. Thus, if the P–E loop drifts to the left, then the P–V drifts to the right, assuming that the space charge is positive and there are more oxygen vacancies near the top surface than the bottom one. Consequently, a positive built-in field exists directing from the top electrode to the bottom one. The drifting direction is reversed if the space charge is negative with the space charge distribution unchanged. Alternatively, the reverse drifting can also be obtained by having more positive space charge at the bottom than at the top. Lee *et al.*[31] have deposited $Pb_{0.9}La_{0.1}Zr_{0.2}Ti_{0.8}O_3$ film between $La_{0.5}Sr_{0.5}CoO_3$ electrodes under 100 mTorr oxygen pressure. The films were then cooled at various oxygen pressures ranging from 10^{-5} to 760 Torr. The P–V loop shifts toward the positive voltage direction on reducing the oxygen pressure and the concentration of oxygen vacancies on the top electrode increases while that at the bottom electrode basically remains unchanged for cooling under the reduced oxygen atmosphere. This result qualitatively agrees with our present model. Friessnegg *et al.*[25] have obtained a similar result. Moreover, their result also indicates a built-in field directing from the top electrode to the bottom one, provided that the layer near the top electrode has more oxygen vacancies.

In addition to the above experimental evidence, there are other results showing that space charge in the oxygen depleted layer in PZT is positive.[18,26,32,33] The oxygen vacancy itself bears a positive charge by releasing electrons. Experimental results also reveal that holes are injected across the electrode film interface,[34] and that oxygen vacancies or their related defect complexes are hole traps.[16,32] If an alternating driving field is applied on the film, it is envisaged that the deep level of a hole trap located in the middle of the band gap is unfilled when the Fermi level is above the deep level during the positive half cycle. On the other hand, holes are injected from the electrode or attracted from the film interior to the space charge region during the negative half cycle. The amount of space charge at the space charge region thus increases. Some of the trapped holes are, of course, released from this deep levels during the other positive half cycle by hole emission when the Fermi level is raised above the deep level again. It is believed that the trapping of holes by these deep levels is more efficient than the detrapping. It then results in a net gain of holes after each switching cycle. This explains why qualitatively the space charge concentration $\tilde{q}_r$ increases with the number of switching cycles N. In order to determine the relation between $\tilde{q}_r$ and N, it is necessary to find the trapping and detrapping rates. These rates can be determined by a standard characterization technique used in semiconductors: deep level transient spectroscopy. To conclude, whether the oxygen vacancy or a complex defect formed by the oxygen vacancy is a hole trap requires further investigation; the associated trapping and detrapping rates must be measured in order to determine the temporal evolution of space charge.

We have assumed that the distribution function is stationary, even though the magnitude of charged oxygen vacancies increases with time by the trapping of holes. In reality, the oxygen vacancy is quite a mobile species in oxide ceramics, especially when a large electric field is present. Thus, the distribution function varies with time. The temporal evolution of the electric field profile not only depends on the time-dependent boundary condition, $\phi(d_z)=V_a(t)$, but also on the time-dependent profile. For a better simulation, it is necessary to determine the time-dependent oxygen vacancy distribution by solving the drift–diffusion equation. The time-dependent space charge concentration is given by the portion of hole-trapping vacancies. This portion depends on the trapping and detrapping rates of the deep level and also on the number of switching cycles. Furthermore, we have only considered the effect of oxygen vacancies at the top or bottom of a perovskite cell on the flipping of a dipole. Assuming that the probabilities of an oxygen vacancy being located on each of the six faces of the cell are equal, then the number of oxygen vacancies located on the vertical walls of the cell must be twice the number of those on the top or bottom faces. As we have mentioned before, Ti^{4+} is restricted in the central plane when an oxygen vacancy is on one of the vertical walls. As a result, there is no dipole switching and no contribution to polarization in this case. Effectively speaking, the volume of the film is reduced by the portion of cells where oxygen vacancies are located at the vertical walls. On the other hand, the charge trapping is independent of the position of the oxygen vacancy in the cell. Thus, the space charge magnitude must be corrected by a factor of 3 in order to cater to the presence of these oxygen vacancies.

IV. CONCLUSION

The roles of oxygen vacancies in perovskite-type ferroelectric thin films have been modeled. In the presence of an oxygen vacancy in a cell, the potential energy for the displacement of the titanium ion becomes asymmetric, displacing favorably to the equilibrium site with lower energy. It

Downloaded 01 Apr 2011 to 158.132.161.9. Redistribution subject to AIP license or copyright; see http://jap.aip.org/about/rights_and_permissions

could possibly displace to the other equilibrium site, with the expense of extra energy. Furthermore, the oxygen vacancy or its related defect complex also traps holes, building up space charges at the two interfaces. The uneven distribution of oxygen vacancies induces the imprint effect. The accumulation of space charges due to trapping results in polarization fatigue.

ACKNOWLEDGMENTS

This work was financially supported by The Center for Smart Materials, Area of Strategic Development of the Hong Kong Polytechnic University (Account No. 1.11.37.A306).

[1] E. L. Colla, A. K. Tagentsev, D. V. Taylor, and A. L. Kholkin, Appl. Phys. Lett. **72**, 2478 (1998).
[2] J. Lee, C. H. Choi, B. H. Park, T. W. Noh, and J. K. Lee, Appl. Phys. Lett. **72**, 3380 (1998).
[3] C. H. Park and D. J. Chadi, Phys. Rev. B **57**, 13961 (1998).
[4] W. L. Warren, D. Dimos, and R. W. Waser, Mater. Res. Bull. **21**, 40 (1996).
[5] H. M. Duiker, P. D. Beal, J. F. Scott, C. A. Pas de Araujo, B. M. Melnice, J. D. Cuchiro, and L. D. McMillan, J. Appl. Phys. **68**, 5783 (1990).
[6] V. M Gurevich, *Electric Conductivity of Ferroelectrics* (Program for Scientific Translations Jerusalem, Israel, 1971), p. 306.
[7] R. Ramesh, H. Gilchrist, T. Sands, V. G. Keramidas, and D. K. Fork, Appl. Phys. Lett. **63**, 3592 (1993).
[8] S. Y. Chen and V. C. Lee, J. Appl. Phys. **87**, 8024 (2000).
[9] H. Geunjo and J. Lee, Surf. Coat. Technol. **131**, 543 (2000).
[10] T. Mihara, H. Watanabe, and C. A. Pas de Araujo, Jpn. J. Appl. Phys., Part 1 **33**, 5281 (1994).
[11] V. C. Lo and Z. J. Chen, Proceedings of the 2000 12th International Symposium on Applications of Ferroelectrics, 27 July – 2 August Honolulu, Hawaii (2000), p. 157.
[12] D. Dimos, H. N. Al-Shareef, W. L. Warren, and B. A. Tuttle, J. Appl. Phys. **80**, 1682 (1996).
[13] S. Maruno, T. Murao, T. Kuroiwa, N. Mikami, A. Tomikawa, T. Nagata, T. Yasue, and T. Koshikawa, Jpn. J. Appl. Phys., Part 2 **39**, L416 (2000).
[14] D. Fuchs, M. Adams, P. Schweiss, S. Gerhold, S. Schuppler, R. Schneider, and B. B. Obst, J. Appl. Phys. **88**, 1844 (2000).
[15] A. Q. Jiang, Z. X. Hu, and L. D. Zhang, Appl. Phys. Lett. **74**, 114 (1999).
[16] P.F. Baude, C. Ye, and D. L. Polla, Appl. Phys. Lett. **64**, 2670 (1994).
[17] M. Dawber and J. F. Scott, Appl. Phys. Lett. **76**, 1060 (2000).
[18] S. B. Desu, Phys. Status Solidi A **151**, 467 (1995).
[19] A. S. Carrico, C. A. Pas de Araujo, T. Mihara, and H. Watanabe, Integr. Ferroelectr. **13**, 247 (1996).
[20] A. Chen and Y. Zhi, Phys. Rev. B **62**, 228 (2000).
[21] K. P. Lee, S. J. Kang, and Y. P. Yoon, J. Inst. Electr. Eng. Korea SD **37-SD**, 24 (2000).
[22] S. Maruno, T. Kuroiwa, M. Mikami, K. Sato, S. Ohmura, K. Kaida, T. Yasue, and T. Koshikawa, Appl. Phys. Lett. **73**, 954 (1998).
[23] S. M. Wang, *Computational Methods in Physics and Engineering*, 2nd ed., (World Scientific, Singapore, 1992), p. 342.
[24] S. W. Sides, P. A. Rikvold, and M. A. Novotny, Phys. Rev. E **59**, 2710 (1999).
[25] T. Friessnegg, S. Aggarwal, R. Ramesh, E. H. Nielsen, and D. J. Keeble, Appl. Phys. Lett. **77**, 127 (2000).
[26] B. H. Park, T. W. Noh, K. P. Lee, C. Y. Kim, and W. Jo, Appl. Phys. Lett. **70**, 1101 (1997).
[27] A. M. Bratkovsky and A. P. Levanyuk, Phys. Rev. B **61**, 15042 (2000).
[28] S. R. P. Smith, J. Phys.: Condens. Matter **10**, 9141 (1998).
[29] A. K. Tagantsev, Integr. Ferroelectr. **16**, 237 (1997).
[30] H. N. Al-Shareef, D. Dimos, T. J. Boyle, W. L. Warren, and B. A. Tuttle, Appl. Phys. Lett. **68**, 690 (1996).
[31] J. Lee, R. Ramesh, V. G. Keramides, W. L. Warren, G. E. Pike, and J. T. Evans, Appl. Phys. Lett. **66**, 1337 (1995).
[32] H-M. Chen and J. Y-M. Lee, J. Appl. Phys. **82**, 3478 (1997).
[33] D. J. Wouters, G. J. Willems, and H. E. Maes, Microelectron. Eng. **29**, 249 (1995).
[34] I. Stolichnov and A. Tagantsev, J. Appl. Phys. **84**, 3216 (1998).

Downloaded 01 Apr 2011 to 158.132.161.9. Redistribution subject to AIP license or copyright; see http://jap.aip.org/about/rights_and_permissions